High-Reynolds Number Solutions of Incompressible Navier-Stokes Equations using Vectorial Operator Splitting

Rossitza Marinova[1], Christo Christov[2], and Tchavdar Marinov[3]

[1] Varna Free University, Varna 9007, Bulgaria
[2] University of Louisiana at Lafayette, Lafayette, LA 70504-1010, USA
[3] Saitama Institute of Technology, 1690, Fusaiji, Okabe, Saitama 369-0293, Japan

Abstract. The steady incompressible Navier-Stokes equations in primitive variables are solved by implicit vectorial operator-splitting. The method allows for complete coupling of the boundary conditions. Conservative approximations for the advective terms are employed on irregular staggered grids. The technique is used here for solving two benchmark problems. Numerical solutions for the flow in a lid-driven rectangular cavity with aspect ratio two (up to $Re = 6000$) and for the flow over backward-facing step in a channel (up to $Re = 1400$) on appropriate grids are presented.

1 Introduction

Consider the steady incompressible Navier-Stokes equations with equation for pressure instead the continuity equation (see [2,3] for details)

$$\frac{1}{Re}\Delta \boldsymbol{u} - \boldsymbol{\nabla} p - C[\boldsymbol{u}] = 0 \,, \quad \frac{1}{Re}\Delta p - \boldsymbol{\nabla}\cdot\boldsymbol{u} + \frac{1}{Re}\boldsymbol{\nabla}\cdot C[\boldsymbol{u}] = 0 \tag{1}$$

in a closed domain Ω with a piece wise smooth boundary $\partial\Omega$. Here $\boldsymbol{x} \in \Omega$, $\boldsymbol{u} = \boldsymbol{u}(\boldsymbol{x})$ is the velocity vector, $p = p(\boldsymbol{x})$ – the pressure. The Reynolds number is defined as $Re = UL/\nu$, where U is the characteristic velocity, L – characteristic length, ν – kinematic coefficient of viscosity. The operator $C[\boldsymbol{u}]$ is a short-hand notation for the advective term. For this term we use the skew-symmetric form

$$C[\boldsymbol{u}] = \boldsymbol{\nabla}\cdot(\boldsymbol{u}\boldsymbol{u}) - \frac{1}{2}\boldsymbol{u}(\boldsymbol{\nabla}\cdot\boldsymbol{u}) \,, \tag{2}$$

which follows from the continuity equation.

We assume that the velocity components are prescribed at the boundaries. The formulation with the equation for pressure is equivalent to the original system only if the continuity equation is satisfied also on the boundary [2,8]. Therefore we take

$$\boldsymbol{u}\big|_{\partial\Omega} = \boldsymbol{u}_b \,, \quad \boldsymbol{\nabla}\cdot\boldsymbol{u}\big|_{\partial\Omega} = 0 \,. \tag{3}$$

For incompressible flows the pressure is defined up to an arbitrary function of time. For the sake of convenience we define this function as the average of the pressure at the specific time stage, i.e., we assume (for pressure uniqueness) that the following relation is satisfied $\int_\Omega p(\boldsymbol{x},t)\mathrm{d}\boldsymbol{x} = 0$, $\boldsymbol{x} \in \Omega$, $t > 0$.

N. Satofuka (ed.), *Computational Fluid Dynamics 2000*

In this work we consider two-dimensional case only. Upon introducing fictitious time t we arrive at the following vectorial parabolic system

$$\frac{\partial \boldsymbol{\theta}}{\partial t} = L[\boldsymbol{\theta}] + N[\boldsymbol{\theta}] + F[\boldsymbol{\theta}] , \quad \text{where} \quad \boldsymbol{\theta} = \begin{pmatrix} u \\ v \\ p \end{pmatrix} ,$$

$$L = \begin{pmatrix} \Delta/Re & -\nabla & 0 \\ 0 & \Delta Re & -\nabla \\ -\nabla & -\nabla & \Delta/Re \end{pmatrix} , N = -\begin{pmatrix} C & 0 & 0 \\ 0 & C & 0 \\ 0 & 0 & 0 \end{pmatrix} , F[\boldsymbol{\theta}] = \begin{pmatrix} 0 \\ 0 \\ (\nabla \cdot C[\boldsymbol{u}])/Re \end{pmatrix} .$$

Solving this problem numerically is a formidable task in the case of high Reynolds numbers. The proposed vectorial version of the operator-splitting implicit scheme preserves the coupling between the sought functions at each fractional-time step.

2 Vectorial Operator-Splitting

We employ the second Douglas scheme [4] which is sometimes called "stabilizing correction". It is of first order in time, but has some advantages in stability, especially for non-commuting operators [10]. The order of approximation with respect to the fictitious time is not important here as far as we are looking for the stationary solution after the time stepping (iterations) converges. The two steps of the scheme of stabilizing correction are

$$\frac{\widehat{\boldsymbol{\theta}} - \boldsymbol{\theta}^n}{\tau} = A_1 \widehat{\boldsymbol{\theta}} + A_2 \boldsymbol{\theta}^n + G^n , \quad \frac{\boldsymbol{\theta}^{n+1} - \widehat{\boldsymbol{\theta}}}{\tau} = A_2 (\boldsymbol{\theta}^{n+1} - \boldsymbol{\theta}^n) , \tag{4}$$

τ is the increment of the fictitious time. The half-time-step variable $\widehat{\boldsymbol{\theta}}$ can be eliminated from (4) to get

$$(I + \tau^2 A_1 A_2) \frac{\boldsymbol{\theta}^{n+1} - \boldsymbol{\theta}^n}{\tau} = (A_1 + A_2) \boldsymbol{\theta}^{n+1} + G^n . \tag{5}$$

It is seen that upon convergence, i.e. $||\boldsymbol{\theta}^{n+1} - \boldsymbol{\theta}^n|| \to 0$, the solution of the evolution problem satisfies the steady problem and the order of approximation does not depend on τ.

We treat implicitly the nonlinear operators, i.e., $A_1 = L_1 + N_1$, $A_2 = L_2 + N_2$. Here L_1 and L_2 are the operators of the derivatives with respect to x and y of the operator $L = L_1 + L_2$. Respectively N_1 and N_2 are the operators of the derivatives with respect to y and x of the operator $N = N_1 + N_2$.

We select a mesh which is non-uniform and staggered in x-direction for u and in y-direction for v. For boundary conditions involving derivatives this allows one to use central differences with second-order of approximation on two-point stencils. We employ difference approximations for the derivatives, which inherit the properties of the respective differential operators.

The gist of the new scheme is that it allows a special treatment of the algebraic systems. One of the systems for the respective velocity component is

always conjugated to the system for pressure set function. For instance, on the first half-time stage the x operators are inverted along the line $y = y_j$ when u and p are conjugated. Then two linear algebraic systems are to be solved: one with tridiagonal matrix for v, and another (a conjugated one) – for the "composite" difference function obtained from the special arrangement of the two functions u and p. The latter has a pentadiagonal matrix twice the size of the tridiagonal one. In the same manner, the second half-time step requires to solve a tridiagonal and a pentadiagonal system.

The proposed difference scheme and algorithm are robust for large values of Reynolds number. To illustrate the advantages of the new method we conduct numerical tests for two different benchmark problems using uniform and/or non-uniform grids. Three grids are used in our computations. All computations are done with tolerance 10^{-10} for the criterion of convergence in terms of the normalized residual vector.

3 Lid-Driven Flow in Rectangular Cavity

Computational results for Reynolds number up to 11,000 for the flow in square cavity can be found in [3]. Here we consider rectangular cavity with aspect ratio 2. In studying this flow our aim is to verify that the scheme is able to determine the solutions in such a geometry for large enough Reynolds number. Steady solutions for this flow are presented in [1,6].

The streamlines of the solution obtained using Richardson extrapolation of the solutions with $h = 1/256$ and $h = 1/512$ for $Re = 1000$ and 6000 are plotted in Fig. 1. There are differences between our results and the results in [1] in the lower part of the cavity. Probably it is due to the presence of instabilities during iterations in [1]. The bottom-right and bottom-left secondary vortices are more intensive in our work comparing with [6]. The data concerning the location and

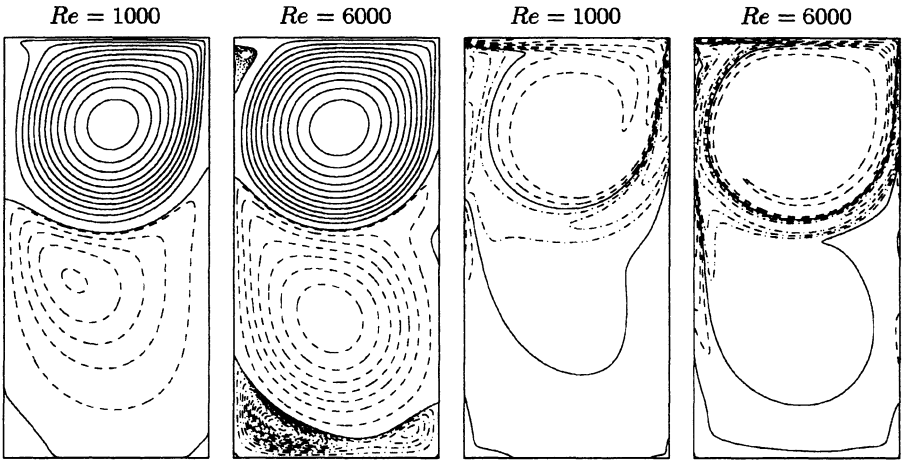

Fig. 1. Streamlines (left) and vorticity isolines (right) for $Re = 1000$ and $Re = 6000$

Table 1. Coordinates of the extrema of the stream function: Pr. – present results; R256 – Richardson extrapolation from solutions with $h = 1/256$ and $h = 1/512$

Re	Ref.	$1/h$	Primary Top Vortex		Primary Bottom Vortex	
	data		$\psi_{\min}$	$(x_{\min}, y_{\min})$	$\psi_{\max}$	$(x_{\max}, y_{\max})$
1000	[1]	256	−0.1169	(0.5273, 1.5625)	0.0148	(0.3516, 0.7891)
	[6]	256	−0.1187	(0.5313, 1.5781)	0.0132	(0.3359, 0.8476)
	Pr.	R256	−0.117945	(0.5299, 1.5795)	0.013330	(0.3424, 0.8379)
6000	Pr.	R256	−0.119759	(0.5147, 1.5645)	0.021418	(0.4694, 0.6612)

strengths of the primary top vortex and the primary bottom vortex in the flow are presented in Table 1. Our results for $Re = 1000$ are compared with those in [1,6]. For $Re > 1000$ we were unable to find any steady state benchmark solution for comparisons. Therefore we present only our results.

4 Flow over a Backward-Facing Step in a Channel

Consider the flow over a backward-facing step, which is another well-studied test case. Fig. 2 shows the geometry of the flow and the defined flow parameters. Steady state numerical solutions are obtained up to $Re = 800$ in a fairly large number of works, see [5,7,9]. The Reynolds number is based on the mean inflow velocity U, the channel height H, and the viscosity ν. On the walls of the channel no-slip boundary conditions are used. At the inlet boundary ($x = 0$, $h \le y \le H$) a parabolic profile $u = 6U(H-y)(y-h)/(H-h)^2$, $v = 0$ is prescribed. The outflow velocity profile is also taken to be parabolic $u = 6U(H-y)y/H^2$, $v = 0$.

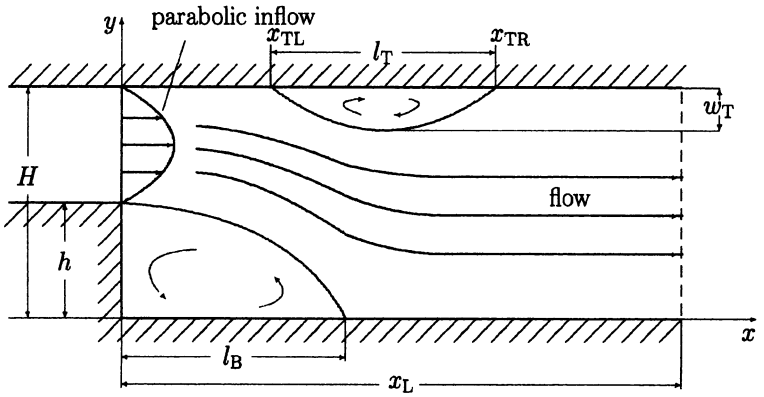

Fig. 2. Geometry of the flow over a backward-facing step in a channel ($h : H = 1 : 2$)

Table 2. Comparison of characteristic flow parameters for $Re = 800$, $H = 1$

Ref.	l_B	l_T	x_{TL}	x_{TR}	ψ_{min}	ψ_{max}	Nodes
[5]	6.10	5.63	4.85	10.48	−0.0342	0.5064	129681
[7]FD	6.082	5.6260	4.8388	10.4648	−0.034195	0.50661	245760
[9]	6.0964	5.6251	4.8534	10.4785	−0.03420	0.50653	3737
Pr.	6.0909	5.6505	4.8214	10.4719	−0.03421	0.50653	Extr.

Our tests have shown that for $Re \leq 1400$ it is safe to take $x_L \approx 100h$. The grid is non-uniform with numbers of the sells for the coarsest grid (Grid 1) in x and y direction $N_x = 256$ and $N_y = 64$, respectively. The grid in x-direction is denser near the walls, while near the outlet boundary lesser number of grid

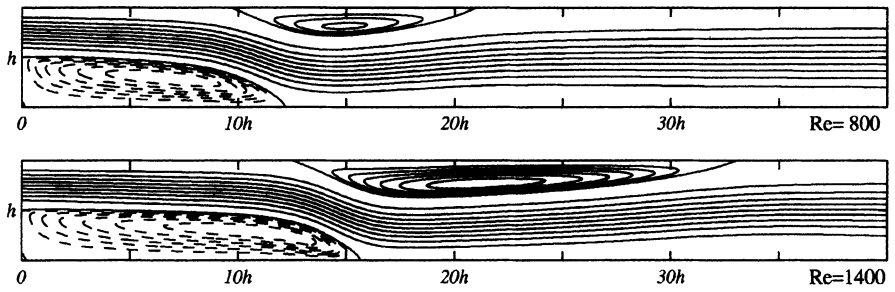

Fig. 3. Streamlines (expansion ratio 1:3)

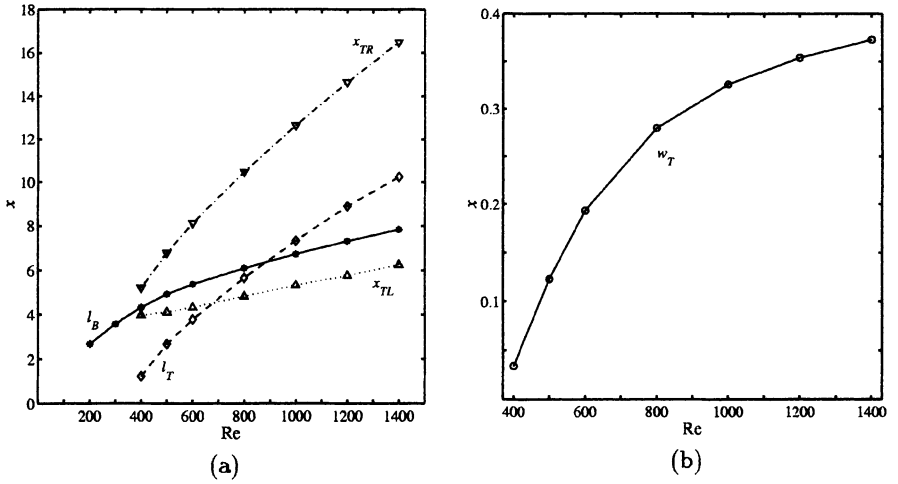

Fig. 4. Variation in different flow characteristics with Re: (a) reattachment and separation lengths ($*$ – l_B; $\diamond$ – l_T; $\triangle$ – x_{TL}; ∇ – x_{TR}); (b) width w_T of the upper eddy

lines are used. In the interval $[0, x_c]$, where $x_c > x_{TR}$, a fine uniform grid is employed with number of grid cells $N_c = 7(N_y - 1)/8$. The finer grid (Grid 2) is constructed on the base of of the coarse Grid 1 through adding a middle point between two grid points. In a similar fashion, the finest grid (Grid 3) is constructed on the basis of Grid 2. Finally, using the obtained solutions on the last two grids, a Richardson extrapolation is performed and the accuracy of the solutions is increased to fourth order. We have obtained the steady solutions on all grids except for $Re = 1400$ on Grid 1. For the highest Reynolds number, convergence could not be reached on the course Grid 1.

Fig. 3 shows the streamline plots for $Re = 800$ and $Re = 1400$. In Table 2 the values of reattachment lengths l_B, l_T are presented as well as the longitudinal positions x_{TL}, x_{TR}, respectively of the start and end of the upper eddy. Our computations for $Re = 800$ are compared with benchmark computations of [5,7,9]. In Fig. 4, the obtained computational results of the most representative characteristics of the flow as function of the Reynolds number are shown. Our results for l_B are close to those in many other works for Reynolds number up to 800. Up to $Re = 1400$ our calculations show that the appearance of the upper eddy slows down the growth of the bottom eddy, see Fig. 4–(a). For Reynolds number $Re \geq 600$ the dependence of the reattachment length l_B on Re is almost linear with a less slope than those for $Re \leq 400$. Our computation shows that the length of the upper eddy l_T grows faster than l_B. For some value of $Re \leq 900$ the length l_T becomes longer than the length of the bottom eddy l_B. Fig. 4–(b) shows the dependence of the width of the secondary eddy w_T on Reynolds number.

Acknowledgements

The work of C.C. is supported in part by Grant LEQSF(1999-2002)-RD-A-49 from the Louisiana Board of Regents. The support for T.M. from the JSPS under Grant No P99745 is gratefully acknowledged.

References

1. C.-H. Bruneau, C. Jouron: J. Comput. Phys. **89**, pp. 389–413 (1990)
2. C. I. Christov, R. S. Marinova: 'Implicit vectorial operator splitting for incompressible Navier–Stokes equations in primitive variables'. Submitted to: Comput. Methods Appl. Mech. Engn.
3. C. I. Christov, R. S. Marinova: 'Implicit scheme for Navier–Stokes equations in primitive variables via vectorial operator splitting'. In: *Notes on Numer. Fluid Mech. 62*, ed. by M. Griebel et al. (Vieweg, Wiesbaden 1998) pp. 251–259
4. J. Douglas: SIAM Journal **3**, pp. 42–65 (1955)
5. D. Gartling: Int. J. Numer. Meth. Fluids **11**, pp. 953–967 (1990)
6. O. Goyon: Comput. Meth. Appl. Mech. Engrg. **130**, pp. 319–355 (1996)
7. P. M. Gresho et al: Int. J. Numer. Meth. Fluids **17**, pp. 501–541 (1993)
8. A. D. Henshaw: J. Comp. Phys. **113**, pp. 13–35 (1994)
9. Jayant Keskar, D. A. Lyn: Int. J. Numer. Meth. Fluids **29**, pp. 411–427 (1999)
10. N. N. Yanenko: *Method of fractional steps* (Gordon and Breach, New York, 1971)